small NANO MICRO

Fluorescent Labels

Bioconjugated Fluorescent Zeolite L Nanocrystals as Labels in Protein Microarrays

*Zhen Li, Gianluigi Luppi, Albert Geiger, Hans-Peter Josel, and Luisa De Cola**

Zeolite L nanocrystals, as inorganic host material containing hydrophobic fluorophore N,N′-bis(2,6-dimethylphenyl)perylene-3,4,9,10-tetracarboxylic diimide in the unidirectional channels, are developed as new labels for biosensor systems. The external surface of the particles is modified with carboxylic acid groups for conjugation to primary amines of biomolecules such as antibodies. Anti-digoxigenin (anti-DIG) is selected to be immobilized on zeolite L via N-hydroxysulfosuccinimide ester linker. Together with DIG, it serves as a good universal binding pair for diverse analyte detection owing to the high binding affinity and low background noise. The conjugates are characterized by the dynamic light scattering technique for their hydrodynamic diameters and by enzyme-linked immunosorbent assay for antigen–antibody binding behavior. The characterizations prove that anti-DIG antibodies are successfully immobilized on zeolite L with their binding activities maintained. The microarray fluorescent sandwich immunoassay based on such nanocrystalline labels shows high sensitivity in a thyroid-stimulating hormone assay with the lower detection limit down to the femtomolar range. These new fluorescent labels possess great potential for in vitro diagnostics applications.

1. Introduction

Increasing research and development of protein arrays has opened a new era of in vitro diagnostics.[1] Short turnaround time, small sample volumes, lower detection limits, and multiparameter analysis can all be realized on a microchip several square millimeters in size.[2,3] In addition, Gygi et al. have demonstrated the lack of correlation between gene transcripts and protein abundance, which proves that the microarray at the proteomic level is an important complementary tool to the DNA array.[4] Together with biostatistical methods, it results in a powerful combination for monitoring and assessments of patient health status, environment, drug development, and improved therapy. However, compared to DNA arrays, the protein microarray has more complex coupling chemistry, problems with instability of the immobilized protein, and weaker detection signals (e.g., antibody–antigen interactions).[5,6] Therefore, the selection of a suitable assay system becomes an important issue for the detection of proteins at low concentration.

To achieve this goal, two main factors should be taken into consideration. The first is the immunological system involved. To be more specific, the binding affinity of the antibody–antigen pair has to be high, especially in complex assay applications. Besides the well-known universal bioanalytical binding partner avidin or streptavidin and biotin, anti-digoxigenin (anti-DIG) and digoxigenin (DIG) has been introduced owing to the relatively high binding constant and good signal-to-noise ratio.[7,8] The second factor is the sensitivity of the detection system. Recently, several materials have been developed in this emerging field, such as gold nanoparticles, quantum dots, and core/shell silica nanoparticles.[9–14] Also, it has been shown that antibodies can be coupled on magnetic nanoparticles,[15,16] mesoporous silica,[17–19] metallic particles, and nanocomplexes.[20–22]

Dr. Z. Li, Dr. G. Luppi, Prof. L. De Cola
Physikalisches Institut and Center for Nanotechnology, CeNTech
Universität Münster
Heisenbergstr. 11, 48149 Muenster, Germany
E-mail: decola@uni-muenster.de
Dr. A. Geiger, Dr. H.-P. Josel
Roche Diagnostics GmbH
Nonnenwald 2, 82377 Penzberg, Germany

DOI: 10.1002/smll.201100959

Since the signal-to-noise ratios of photomultiplier tubes and charge-coupled device (CCD) cameras are very low, fluorescent labels are still one of the most sensitive detection systems in many applications. However, with organic fluorescent molecules the sensitivity is limited due to the label density on the antibody. To overcome this problem, several dye-doped nanoparticles have been developed, in particular based on silica particles.[23,24] Tan et al. have demonstrated that enzyme modification of silica-based nanoparticles used as a biosensor resulted in good biocompatibility and excellent enzymatic activity.[25]

Herein, we describe new fluorescent labels, based on inorganic nanocrystalline zeolite L, for low-concentration analyte applications in microarrays. Zeolite L is a synthetic aluminosilicate with a Si/Al ratio of typically 3.0, which consists of unidimensional nanochannels with an opening diameter of 0.71 nm and cavities of $0.48 \times 1.24 \times 1.07$ nm.[26,27] The channels can host fluorophores which can be organized along a defined direction.[28–33] These fluorophores are also protected by the environment and have a low aggregation tendency.[34] Furthermore, the external surface can be modified with several functional groups, and the functionalization can be spatially resolved so that different groups at the channel entrances and on the coating can be covalently attached.[35–38] This functionalization can also improve the biocompatibility of the zeolites, which are used to connect living organisms and we have recently demonstrated that we can use these materials to target,[39] label, and kill bacteria.[40] Recently, we have also shown that, with an appropriate filling of the channels in combination with surface functionalization, the nanocrystals can be used for in vivo imaging.[41] Zeolites L have been used as microreactors in a proteolysis system as well as to selectively adsorb biopolymers.[42,43] In our approach we synthesized disc-shaped zeolite L nanocontainers using a modified procedure[44] (see Experimental Section) and loaded them by a gas-phase process with the green-emitting fluorophore *N*,*N*′-bis(2,6-dimethylphenyl)perylene-3,4,9,10-tetracarboxylic diimide (DXP) as potential label.[45] Anti-DIG antibodies were conjugated on the surface of the crystals and the hybrid systems were employed in microarray fluorescence immunoassay for the detection of thyroid-stimulating hormone (TSH). These functional nanocrystals show high potential as fluorescent labels in array technology.[46]

2. Results and Discussion

2.1. Zeolite L Synthesis and External Surface Activation

According to the hydrothermal procedure described in the literature,[44] disc-shaped zeolite L crystals were successfully synthesized that possessed an average hydrodynamic diameter of around 195 nm with a polydispersity index (PDI) of 0.13 (see Supporting Information Figure S1). The morphology was confirmed by scanning electron microscopy (SEM) analysis as shown in **Figure 1**a and b, in which the

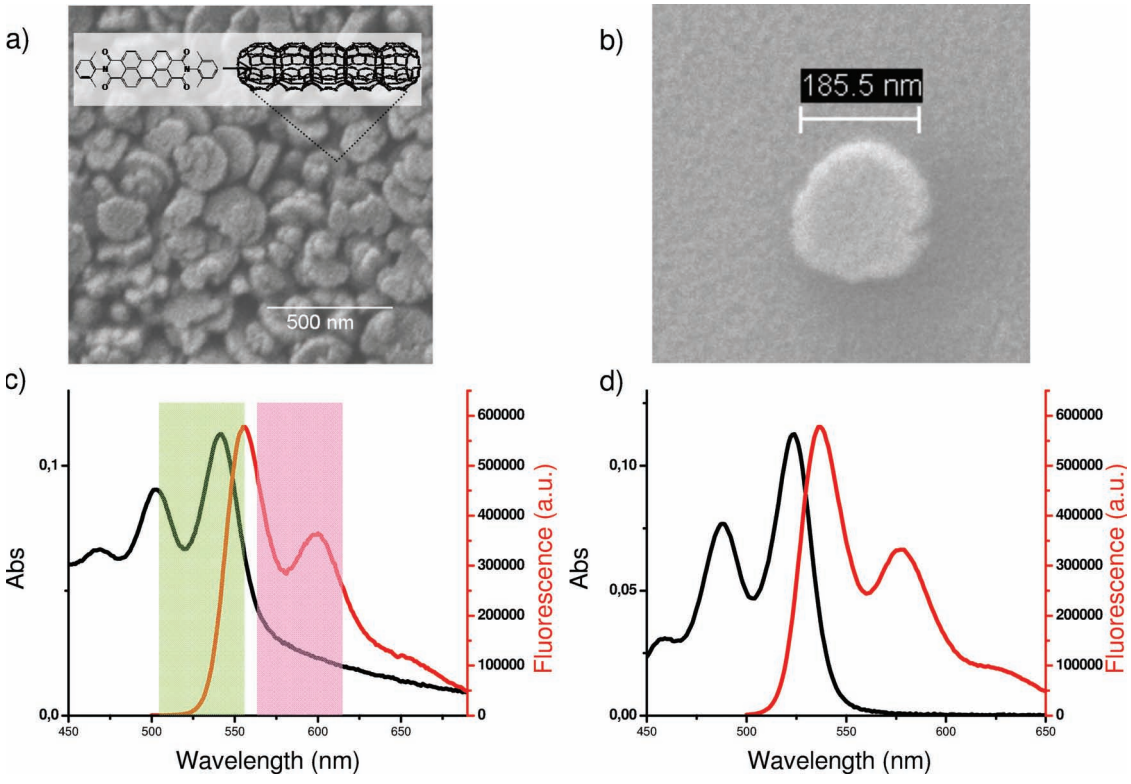

Figure 1. a,b) SEM images of nanodisc-shaped zeolite L. The inset in (a) shows a schematic drawing of zeolite nanochannels filled with DXP. c) Absorption (black line) and emission spectra (red line, exc. = 491 nm) of DXP-loaded zeolite L. The excitation band (green) and emission band (pink) of the equipment filter pair are shown to match the normalized spectroscopic absorption and emission spectra of DXP-loaded zeolite L at the concentration 0.1 mg mL^{-1} in physiological solution. d) Normalized absorption and emission spectra (exc. = 491 nm) of DXP in ethanol for comparison at concentration 5×10^{-6} mol L^{-1}.

NANO MICRO small

size ranges between 170 and 230 nm and the height ranges between 60 and 70 nm. The characteristic X-ray diffraction (XRD) spectra are provided in the Supporting Information, Figure S1. Theoretical calculations show that a particle of 180 nm possesses 925 600 unit cells and gains high potential as a nanocontainer to accommodate fluorescent dyes. In our application, we chose the green emitter DXP as guest molecules to be inserted in the channels of the nanocrystals. DXP was selected because of its suitable molecular size and strong hydrophobicity, thereby avoiding dye leakage into the buffer solution during conjugation, storage, and assay performance.

The excitation and emission spectra are also appropriate for the filter system commonly used in the microarray analysis (excitation = 527 ± 35 nm, emission = 590 ± 35 nm, see Figure 1c). The fluorescent dyes were brought into zeolite channels by gas-phase insertion.[44,45] In particular, calculated amounts of DXP and zeolite L were dehydrated under high-vacuum conditions and kept at sublimation temperature for 48 h. We achieved loadings of about 7%, when considering occupied unit cells against total available ones, which should not result in visible aggregation phenomena inside zeolite L channels, in agreement with what we have reported previously.[45] The loaded zeolites upon excitation at 491 nm show absorption and emission bands (Figure 1c) with spectral features comparable to those obtained in pure ethanol even if slightly red-shifted (see Figure 1d and Supporting Information Figure S2). The emission quantum yield of the DXP in the zeolites was 27% in physiological solution and the excited-state lifetime was 3.7 ns.

Since silanol groups on the external surface of zeolite L are not active enough to react with antibodies, it is necessary to perform additional functionalization steps. Primary amine groups were introduced on the surface by silanization with 3-aminopropyltriethoxysilane (APTES). They subsequently reacted with glutaric anhydride by a ring-opening reaction to form carboxylic acid groups, as illustrated in **Scheme 1**a.

The different particle surfaces were characterized by zeta potential measurements. Suspensions in phosphate-buffered saline (PBS) showed that the zeta potential increased from –39 mV for plain zeolite to +25 mV for the amino-modified particles followed by a decrease to –50 mV after carboxylation, which indirectly proves that the surface has been functionalized since the total charge changes after each functionalization step. Furthermore, surface primary amine groups were quantified by the ninhydrin test (for the calibration curve, see the Supporting Information Figure S3). Different concentrations of APTES were applied as standards in amine concentration calibration curves. The results obtained following the ninhydrin test showed that surface coverage of primary amine per weight of zeolite was 1.14 μmol mg^{-1} (5×10^8 molecules per crystal), while after carboxylic modification there were no detectable amounts of free primary amines left. The external surface of zeolite L nanocrystals was completely modified for the antibody immobilization.

2.2. Zeolite L and Anti-DIG Conjugation

Carboxylic groups were activated by sulfo-NHS ester formation via EDC to target accessible primary amines on antibodies as depicted in Scheme 1b.[47–49] The studies showed that NHS ester activation was recognized as a straightforward and a very efficient route for bioconjugation without impairing the antibody function.[50,51] In our experiment, we use polymerized anti-DIG antibodies with a size of about 20 to 30 nm instead of monomer antibodies. It is well known that antibodies that are covalently attached to solid supports may lose their specific binding capacity in comparison to the free ones in solution. The reason could be the constrained random orientation of antibodies with limited accessibility in comparison to unattached antibodies. In the worst case, Fab (fragment antigen binding) regions would attach to the solid surface facing down and with complete loss of their antigen-binding properties. To eliminate this drawback, anti-DIG antibodies were polymerized with homobifunctional crosslinker

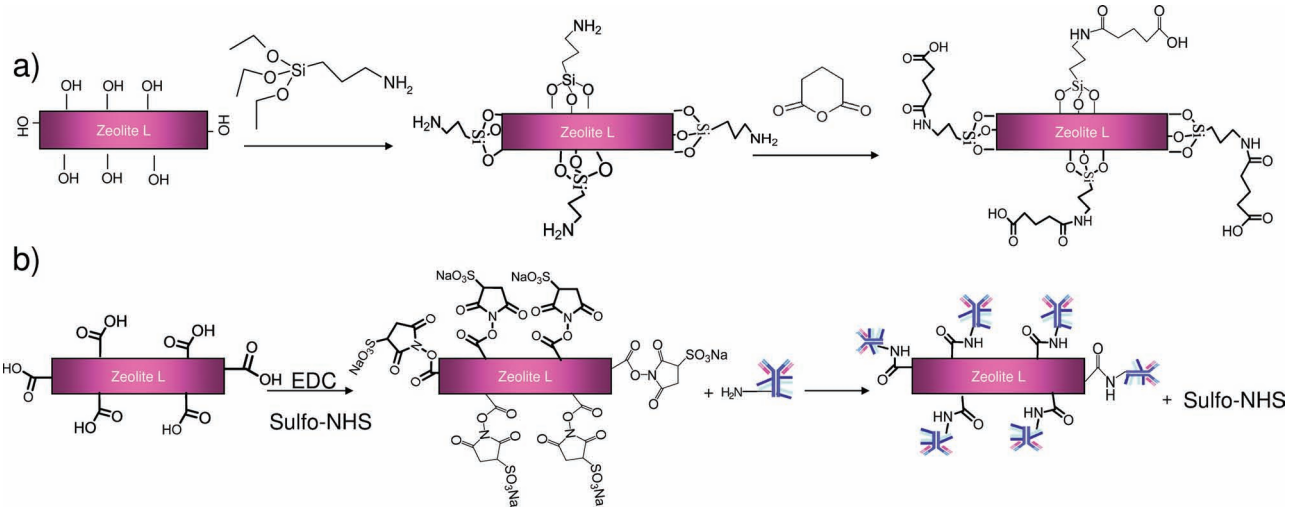

Scheme 1. a) Preparation of carboxylic acid-functionalized zeolite nanoparticles via amino functionalization as intermediates. b) Conjugation reaction of zeolite L and antibody via *N*-hydroxysulfosuccinimide (sulfo-NHS) ester linker coupled by 1-ethyl-3(3-dimethylaminopropyl) carbodiimide hydrochloride (EDC).

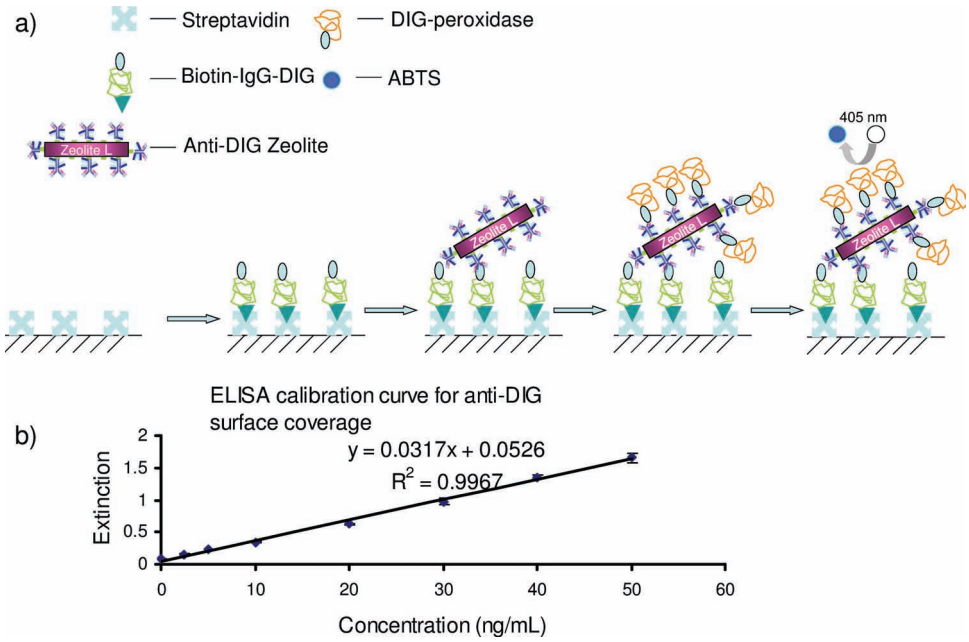

Figure 2. a) Schematic illustration of the general procedure of ELISA tests for active antibodies. DIG was immobilized on a streptavidin-modified surface via biotinylated DIG immunoglobulin G (IgG) conjugates. Conjugated zeolite L nanocrystals were captured in the well through anti-DIG and DIG interaction. The rest of the active anti-DIG on the zeolite surface was titrated by DIG–peroxidase (POD) and followed by absorption change of the POD substrate ABTS at 405 nm. b) ELISA calibration curve to calculate anti-DIG coverage on the zeolite surface in suspension and supernatant.

disuccinimidyl suberate (DSS) before zeolite conjugation to maintain their binding sites accessible after immobilization on nanoparticles and to increase the stability.[52] These crosslinked antibodies have an estimated size of around 20 to 30 nm and were applied as received from Roche Diagnostics. The hydrodynamic diameters of the zeolite nanoparticles measured by dynamic light scattering grew by about 28 nm after conjugation, which was consistent with the size of polymerized antibodies (see Supporting Information Figure S4). This was one piece of evidence that antibodies were attached on the zeolites. However, for our studies only the surface binding sites of antibodies accessible for antigens and defined as active antibodies are important. Their total amount on the nanoparticles was determined by the enzyme-linked immunosorbent assay (ELISA) experiments shown in **Figure 2**.

In these experiments, streptavidin-modified 96-well transparent microtiter plates were applied to measure and calculate anti-DIG concentrations in suspension and supernatant by monitoring the absorption at 405 nm of the POD–2,2′-azinobis(3-ethylbenzthiazoline sulfonate) (ABTS) marker enzyme substrate reaction (see Figure 2a). In this assay, DIG was immobilized on the streptavidin surface by DIG–biotin–IgG conjugates via biotin streptavidin recognition. With an amount of 10 ng of such conjugates per well, it provided a reasonable attachment capacity for further binding to anti-DIG-conjugated zeolite or free anti-DIG in the case of the calibration curve. Zeolites were immobilized on the surface of wells by anti-DIG and DIG interaction. In the next step, the remaining active anti-DIG antibodies formed complexes with DIG–POD conjugates. The surface antibodies were then quantified via an enzyme substrate reaction between POD and ABTS, by monitoring the absorption intensity of ABTS at 405 nm. Based on these results, active anti-DIG antibodies were indirectly calculated against the standard concentration curve. In the experiment, we applied different concentrations of anti-DIG antibodies in solution to determine the calibration curve in order to calculate the unknown concentration of bound antibodies on the zeolite. The calibration curve showed very good linearity from 2.5 to 50 ng mL^{-1} (see Figure 2b). Although we covalently anchored the antibodies on the zeolite nanocrystals, it was still possible that small amounts of unbound antibody molecules remained in suspension. These would compete with bound antibody to bind analyte in the microarray immunoassay, which results in unreliable data. The unbound or weakly bound antibodies were obtained from the supernatant by centrifuging the zeolite conjugate suspension. In this case we tested both the conjugate suspension and its supernatant. The active immobilized antibodies on the zeolite were calculated as 357 μg mL^{-1} (about 58 μg mg^{-1} antibody to zeolite ratio), while the concentration of the unbound antibodies in the zeolite conjugate supernatant was 7 μg mL^{-1}. Considering the significant concentration difference between immobilized and unbound antibodies in suspension, there will not be a notable competition from unbound antibodies to influence subsequent microarray assays. Thus, anti-DIG antibodies were successfully conjugated on fluorescent zeolite L nanocrystals.

2.3. Quantitative TSH Detection on Microarrays

For evaluation of zeolite conjugates in a microarray thyroid-stimulating hormone (TSH) assay, a glycoprotein with a molecular weight of 28 900 Da was selected as model analyte. TSH is one of the most sensitive indicators of thyroid function

NANO MICRO small

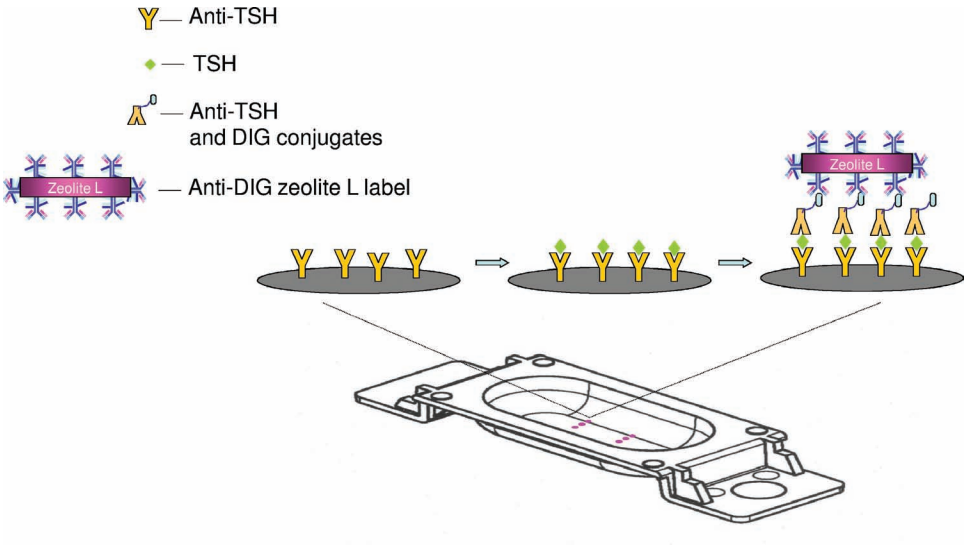

Scheme 2. General representation of TSH immunoassay in a microarray chip. Anti-TSH antibodies were immobilized on the chip surface. TSH was then attached to the chip via antibody–antigen recognition. DIG-bound anti-TSH was linked to the surface by the same type of interaction. Anti-DIG zeolite conjugates then formed a DIG–anti-DIG immunocomplex, thereby immobilizing the fluorescent zeolites on the surface in the presence of TSH.

and therefore has become the most widely tested parameter in the immunodiagnostic market.[53] The ready-prepared microarray chips were designed with four lines of spots where the anti-TSH antibodies as capture molecules were immobilized on the surface for the TSH immunoassay during manufacturing. We used the sandwich immunoassay format on the surface of microarray chips to evaluate the performance of anti-DIG-conjugated zeolite L nanocrystals, as illustrated in **Scheme 2**.

Different concentrations of the analyte TSH (shown in **Table 1**) were applied to the chip, thereby forming a complex with surface-bounded anti-TSH antibodies. DIG-conjugated anti-TSH solution was then added to the chip to allow the recognition of immobilized TSH by the anti-DIG-functionalized fluorescent-dye-loaded zeolite labels. The emission detected upon excitation of the entrapped dye molecules in the zeolites allowed the quantification of the assay. As an example, the emission of different spots on the chip for a fixed concentration of TSH probed by zeolite conjugate label is shown in **Figure 3**a.

To prove that the method is precise and reliable among chips and comparable with the well-known latex bead assay, we repeated one assay with 20 chips keeping the analyte (TSH) concentration at 1.5 μUI mL^{-1}. Results show that the coefficient of variation from chip to chip with 20 repetitions is less than 5% with low background noise (see Supporting Information Table S1). It confirms that the data obtained with zeolite labels were precise and reliable among chips. For further evaluation of the zeolites as labels, eight different concentrations of TSH were tested and the results are summarized in Table 1.

Table 1. Fluorescence intensities of TSH immunoassay and calculated LDL values.[a)]

TSH concentration [μUI mL^{-1}]	Line 1			Line 2			Line 3			Line 4		
	Mean count	SD	CV [%]	Mean count	SD	CV [%]	Mean count	SD	CV [%]	Mean count	SD	CV [%]
control	10.76	3.52	32.74	10.61	3.16	29.81	12.91	2.67	20.68	12.92	1.75	13.53
0.046875	39.46	3.73	9.45	38.72	2.79	7.20	40.32	3.03	7.51	37.10	2.53	6.83
0.09375	39.6	6.02	15.20	38.72	4.99	12.90	40.38	2.77	6.87	37.28	5.02	13.48
0.125	110.68	5.34	4.83	118.02	9.26	7.84	113.22	10.83	9.57	110.66	8.11	7.33
0.1875	229.84	7.02	3.05	238.20	9.42	3.95	224.52	3.28	1.46	211.80	4.26	2.01
0.25	322.76	17.57	5.44	342.72	22.35	6.52	339.70	20.98	6.18	307.88	12.40	4.03
0.375	462.82	26.78	5.79	474.22	21.37	4.51	466.88	19.59	4.20	425.44	21.12	4.97
0.75	1181.46	60.71	5.14	1235.56	72.13	5.84	1171.12	55.82	4.77	1090.94	52.87	4.85
1.5	2374.58	112.32	4.73	2421.22	76.88	3.18	2325.46	61.46	2.64	2220.92	38.01	1.71
LDL [μUI mL^{-1}]	0.0042			0.0038			0.0033			0.0023		

[a)] SD, CV, and LDL represent standard deviation, coefficient of variation, and lower detection limit, respectively. Mean count represents fluorescence intensity.

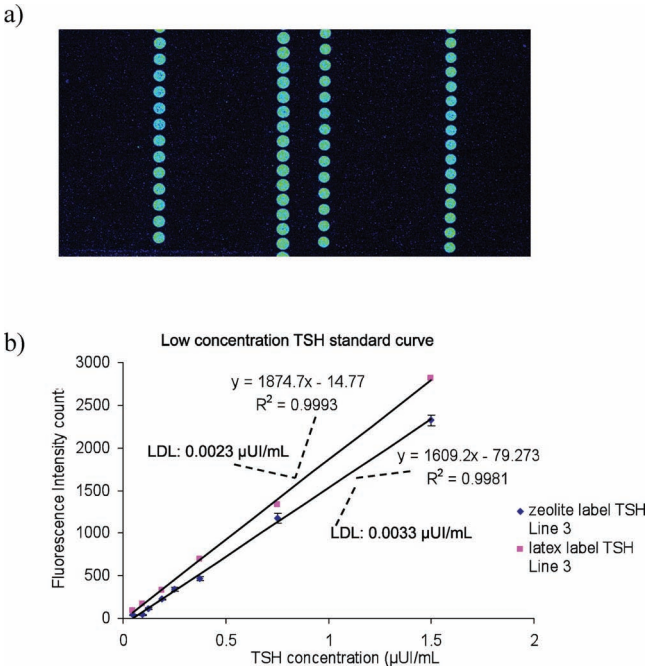

Figure 3. a) Fluorescence images (CCD camera) of protein microarrays after probing by zeolite L nanoparticle labels. The sample had a TSH concentration of 0.75 µUI mL^{-1}. Lines were counted from left to right corresponding to lines 1 to 4 in Table 1. b) TSH assay calibration curves of line 3 on the chips for both fluorescent zeolite and fluorescent latex labels. LDL= lower detection limit.

To quantitatively evaluate an immunoassay, or in other words our fluorescent label, we introduce an important parameter, the lower detection limit (LDL), which is defined as:

$$\mathrm{LDL} = 2 \times S_0/S$$

where S_0 is the standard deviation of the background (here it refers to the SD calculated from samples without analyte but containing all the other notable components, in the absence of the analyte, to form the fluorescent assembly); S is the sensitivity, which can be calculated from the slope of the standard curve (Figure 3b). Therefore, the lower the LDL value the more sensitive is the system. As the concept indicates, two parameters play an important role. The first key issue is that the label should possess a low nonspecific binding to minimize the standard deviation at zero concentration. For zeolite conjugate labels, values of the emission detected in the control samples were very low and spots were hardly seen in the images. The other parameter is the system sensitivity to low analyte concentration variation. In other words, when the assay is very sensitive, the steepness of the slope increases such that the LDL value will decrease. The value determined by this method represents the smallest concentration or quantity that can be distinguished from the blank within a defined level of confidence. We have calculated LDL values based on the data summarized in Table 1 for each four lines in the assay.

Due to the not fully optimized washing procedure on the prototype system for zeolites, small variations of the value for different line positions are observed both in the image and value. The standard calibration curve of line 3 is displayed in Figure 3b as an example. The LDL value is 0.0033 µUI mL^{-1} and the calibration curve shows very good linearity with R^2 (coefficient of determination) equal to 0.999. Considering the size of the conjugated zeolite label and the size of the analyte complex on the chips, it is possible that the single label would cover more than one binding event. However, within the concentration range applied in Table 1, the good linearity ensured the validity of the method. To evaluate our label against the standard fluorescent latex beads that were anti-DIG conjugated, we performed comparative assays under identical conditions (Figure 3b). The results demonstrate that the zeolite labels are, without any optimization, almost as sensitive as the latex beads (latex bead LDL = 0.0023 µUI mL^{-1}). In general, the results for both labels demonstrated that the LDLs of TSH assays are in the femtomolar range with very good linearity.

3. Conclusion

We have proved that zeolite L nanoparticles with encapsulated dye molecules have bright fluorescence properties which can be used for immunoassay quantification. Their external surface can be easily activated and coupled to biomolecules such as antibodies. The ELISA test confirmed that immobilized antibodies retain their binding capability with antigens, which is essential for immunoassay applications. The final evaluation of such a hybrid complex in a protein microarray was performed with TSH as analyte model. Besides low nonspecific binding properties, the LDL of this assay is 0.003 µUI mL^{-1} or at the femtomolar level. These proof-of-principle experiments demonstrate the great potential of zeolite L nanocrystals for applications in high-sensitivity immunoassays in protein microarrays.

4. Experimental Section

Materials: All the antibodies, antigens, enzymes, substrates, oxypyrion, methylisothiazolinone (MIT), bovine serum albumin IV (BSA IV) and StreptaWell (transparent 96-well plate) were obtained from Roche Diagnostics, Penzberg. DXP, *N*-hydroxysulfosuccinimide (sulfo-NHS), 1-ethyl-3(3-dimethylaminopropyl) carbodiimide hydrochloride (EDC), and all the buffers were purchased from Fluka. Polidocanol, aminopropyltriethoxylsilane (APTES), ninhydrin, and Tween 20 were purchased from Sigma–Aldrich. Glutaric anhydride was purchased from ABCR. Dimethyl sulfoxide (DMSO), chloracetamide, dichloromethane (DCM), triethylamine (TEA), and *n*-butanol were purchased from Merck.

Instrumentation: The morphology of the zeolite L nanocrystals was investigated using a Zeiss 1540 EsB dual-beam focused-ion-beam/field-emission scanning electron microscope with a working distance of 8 mm and an electronic high tension (EHT) of 3 kV. Absorption spectra were recorded by a Varian Cary 100 scan UV–visible spectrophotometer. The emission spectra were recorded on a Horiba Jobin-Yvon IBH FL-322 Fluorolog spectrometer equipped with a 450 W xenon arc lamp, double-grating excitation and emission monochromators (2.1 nm mm^{-1} dispersion; 1200 grooves mm^{-1}), and a TBX-4-X single-photon-counting detector (emission). Lifetime was measured using a nano LED laser at 431 nm wavelength

with 1 MHz frequency repetition and 200 ps pulse duration. The absolute quantum yield was measured with a Hamamatsu Photonics K.K. integrated sphere equipped with a 200 W xenon arc lamp, operation wavelength range 200–950 nm, and a BT-CCD linear image sensor with 1024 elements. Dynamic light scattering measurements were performed with a Malvern Zetasizer Nano. Zeta potential was measured with a Malvern Zetasizer 3000HS. ELISA was carried out with a Tecan GENios microplate reader. TSH immunoassay was performed with an automated in-house protein microarray.

Disc-Shaped Zeolite L Synthesis and DXP Insertion: Disc-shaped zeolites were synthesized following the literature procedure with slightly modification.[44] The details of the synthesis procedure are as follows. Potassium hydroxide (2.76 g), sodium hydroxide (1.74 g), and aluminum hydroxide (0.62 g) were added to doubly distilled water (17.40 g) in a round-bottomed flask. The mixture was refluxed for 3 h at 120°C resulting in a clear solution. The solution was cooled to room temperature and then added under stirring to Ludox (17.67 g), which was stirred between 5 and 10 min beforehand. The resulting suspension was stirred for 3 to 6 min. The opaque gel was then transferred to a PTFE vessel and aged for 18 h at room temperature. Crystallization was performed at 160 °C for 48 h under dynamic conditions (rotation at 40 rpm) in an oven. The composition of the gel was 5.40 K_2O–5.50 Na_2O–1.00 Al_2O_3–30.00 SiO_2–416.08 H_2O. After crystallization, the pressure vessel was cooled in an ice bath for 1 h. The product was centrifuged (6000 rpm, 10 min) and washed with boiling doubly distilled water until the pH of the supernatant became neutral. The crystals were dried overnight at 80 °C in an oven to yield about 2 g of material.

Thionine tests and XRD analysis were performed on all synthesized batches (see Supporting Information). DXP dye was used as a fluorescent marker inserted into zeolites by a gas-phase procedure.[45] In a 10-mL ampoule, disc-shaped zeolite (200 mg) was mixed with DXP (1.38 mg, 2.3×10^{-3} mmol) dissolved in dichloromethane (2 mL). The solvent was evaporated under reduced pressure and the homogeneous solid mixture was kept under high vacuum (1×10^{-6} bar) for 8 h. The ampoule was afterwards sealed under vacuum and heated to 300 °C for 48 h with rotation. The excess of DXP in solution and that adsorbed on the external surface of the zeolites was washed away with *n*-butanol and DCM by repeating sonication and centrifugation steps until no luminescence of DXP was observed in the supernatant. The final loading of DXP in zeolite L was determined by HF test. To calculate the DXP final concentration in zeolite L, a certain amount of dye-loaded nanocrystals was dissolved in a HF solution and the absorption spectra of the resulting DXP solution were measured (see Supporting Information).

Preparation of Amino-Functionalized Zeolite L Nanoparticles: Amino zeolites were prepared by sonication of the particles (50 mg) in DMSO (10 mL) for 20 min to form a good dispersion. APTES (100 μL, 0.6 mmol) was added to the suspension in the presence of a catalytic amount of TEA and the mixture was stirred at room temperature overnight. The particles were washed five times with DMSO to remove impurities.

Surface Amino Group Quantification by Ninhydrin Test: Ninhydrin (0.5 g, 2.6 mmol) was dissolved in water-saturated *n*-butanol (10 mL) as stock solution. APTES was diluted in stock solution at concentrations of 0.075, 0.1125, 0.15, 0.1875, and 0.225 μmol mL^{-1}. Amino-functionalized zeolite (0.2 mg) was suspended in stock solution (1.6 mL). Each sample (1.6 mL) was kept at 70 °C for 20 min. The zeolite suspension was centrifuged to obtain the supernatant. After cooling to room temperature, all absorption spectra of supernatants were measured at 570 nm.

Preparation of Carboxylic Acid-Functionalized Zeolite L Nanoparticles: Amino zeolite L was dispersed in DMSO by sonication. After dropwise addition of the suspension to 0.1 M glutaric anhydride in DMSO, the reaction mixture was stirred at room temperature overnight. Excess anhydride was removed by washing with DMSO five times and twice with Millipore water.

Anti-DIG-Coated Zeolite L Nanoparticles: Carboxylated zeolite L nanoparticles were diluted to a 1% (w/v) suspension in 2 mM 2-(*N*-morpholino)ethanesulfonic acid (MES) buffer of pH 6.5 and the mixture was centrifuged. The supernatant was removed and the pellet was resuspended at 2% (w/v) in 2 mM MES buffer at pH 6.5 (note: all buffer exchanges were carried out by centrifugation, removal of the supernatant, and resuspension if not stated otherwise). The suspension (1 mL) was activated by addition of a freshly prepared solution (100 μL) of 2% sulfo-NHS and 0.2% EDC, followed by adjustment of the pH to 6.5 and incubation for 20 min on a roller at room temperature. After centrifugation and removal of the supernatant, the pellet was resuspended in MES buffer (1 mL) as above and sonicated for 10 s. A 2 mg amount of desalted antibody was added per 10 mg of particles. The pH of the reaction mixture was adjusted to 6.5 and it was incubated for 1 h on a roller incubator at room temperature. The conjugation reaction was quenched by addition of 2 M amino compound (30 μL) and the pH was adjusted between 7.5 and 8.5. The mixture was incubated for 30 min on a roller incubator at room temperature. After centrifugation, the pellet was resuspended in 5 mM pH 7.4 PBS buffer (1 mL). After the addition of 2% BSA IV (1 mL) to the suspension, it was incubated for 1 h at room temperature on a roller, and centrifuged. The pellet was resuspended in the same buffer. The same procedure was performed for addition of 1% Tween 20. Afterwards, the mixture was washed twice with the same PBS buffer and finally placed in 5 mM pH 7.4 PBS buffer (0.5 mL). With the addition of 2% BSA IV (0.5 mL), 5% MIT (2 μL), and 5% chloracetamide (52.6 μL), the conjugates were ready for testing. After every centrifugation step, the particle pellet was resuspended with tip sonication in an ice bath for 10 s.

ELISA: Experiments were performed following the instruction manual for DIG Detection ELISA ABTS [2,2′-azinobis(3-ethylbenzthiazoline sulfonate)] kits, which contain streptavidin-coated microtiter plates and DIG–POD for the detection of anti-DIG-conjugated zeolite L nanoparticle suspension and the supernatant. Biotinylated IgG–DIG conjugate (200 μL) was added to a 96-well plate at a concentration of 50 ng mL^{-1}. The plate was incubated for 1 h at room temperature with gentle shaking. For each following step, the microplate was washed with universal buffer by suction after incubation. Different concentrations of anti-DIG antibodies at 0, 2.5, 5, 10, 20, 30, 40, and 50 ng mL^{-1} were applied as calibration curve. Then 10 μL amounts of zeolite conjugate suspension were individually diluted at 1:100, 1:500, and 1:000. After centrifugation of the zeolite conjugate suspension (350 μL), the supernatant (300 μL) was removed as 200, 50, and 50 μL portions. They were further diluted respectively at 1:5, 1:15, and 1:25; 200 μL amounts of each concentration were added to each well with three replicates. The plate was incubated for 1 h at room temperature with gentle shaking for the second time and washed by suction.

DIG–POD solution (200 μL) was added to each well and incubated and washed under the same conditions as before. ABTS solution (200 μL) was added to each well and the plate was kept for 30 min at room temperature. The absorption was measured at 405 nm by a Tecan GENios microplate reader.

TSH Immunoassay: The experiments were performed on an in-house fully automated microarray equipment developed by Roche. Four-line microarray chips were received with immobilized anti-TSH antibodies in the spots. Other reactants, such as zeolite conjugates and different concentrations of TSH, were diluted manually before insertion into the equipment. The zeolite conjugate suspension was diluted to 1 mg mL^{-1} and further diluted to one quarter in the assay process in storage buffer (3.5 mM K_2HPO_4, 1.5 mM KH_2PO_4, 0.01% MIT, 0.25% chloracetamide, 1% BSA IV pH 7.4). TSH solution was prepared at concentrations of 0.046875, 0.09375, 0.1875, 0.375, 0.75, and 1.5 μUI mL^{-1} with five chip replicas for each concentration. For each step, 40 μL solution and 4 min was applied in each chip for incubation. Washing procedures were performed after each step with 100 times diluted washing buffer. Other reactants, such as DIG–anti-TSH conjugates and diverse buffers, were included in the TSH microarray evaluation assay kits. They were obtained from Roche and used as instructed. With the aid of software, fluorescence images taken by CCD camera with filter pair Excitation 527 ± 35 nm and Emission 590 ± 35 nm were converted into signal intensities. The calibration curve was completed for fluorescence intensities versus TSH concentration.

Supporting Information

Supporting Information is available from the Wiley Online Library or from the author.

Acknowledgements

This work was supported by the German Federal Ministry of Education and Research Foundation Grant FZK 03 × 0015 and by the ERC-2009-AdG no. 247365. We thank Roche Diagnostics, Penzberg, for support, G. Geiger for helping with the immunoassays, and D. Furtmair for help with the conjugation procedures.

[1] L. L. Lv, B. C. Liu, *Expert Rev. Proteomics* **2007**, *4*, 505.
[2] M. Ferrari, *Nat. Rev. Cancer* **2005**, *5*, 161.
[3] O. Stoevesandt, M. J. Taussig, M. He, *Expert Rev. Proteomics* **2009**, *6*, 145.
[4] S. P. Gygi, Y. Rochon, B. R. Franza, R. Aebersold, *Mol. Cell. Biol.* **1999**, *19*, 1720.
[5] A. Q. Emili, G. Cagney, *Nat. Biotechnol.* **2000**, *18*, 393.
[6] R. A. Irving, P. J. Hudson, *Nat. Biotechnol.* **2000**, *18*, 932.
[7] Y. Chuang, C.-Y. Lee, S.-H. Lu, S.-C. Wang, L.-K. Chau, W.-H. Hsieh, *Anal. Chem.* **2010**, *82*, 1123.
[8] K. J. Cash, F. Ricci, K. W. Plaxco, *J. Am. Chem. Soc.* **2009**, *131*, 6955.
[9] C. Tortiglione, A. Quarta, A. Tino, L. Manna, R. Cingolani, T. Pellegrino, *Bioconjugate Chem.* **2007**, *18*, 829.
[10] D. Kim, W. L. Daniel, C. A. Mirkin, *Anal. Chem.* **2009**, *81*, 9183.
[11] D. Geissler, L. J. Charbonniere, R. F. Ziessel, N. G. Butlin, H. G. Löhmannsröben, N. Hildebrandt, *Angew. Chem. Int. Ed.* **2010**, *49*, 1396.
[12] M. Montalti, N. Zaccheroni, L. Prodi, N. O'Reilly, S. L. James, *J. Am. Chem. Soc.* **2007**, *129*, 2418.
[13] E. Rampazzo, S. Bonacchi, R. Juris, M. Montalti, D. Genovese, N. Zaccheroni, L. Prodi, D. C. Rambaldi, A. Zattoni, P. Reschiglian, *J. Phys. Chem. B* **2010**, *114*, 14605.
[14] V. Cauda, A. Schlossbauer, J. Kecht, A. Zürner, T. Bein, *J. Am. Chem. Soc.* **2009**, *131*, 11361.
[15] P. Sun, H. Zhang, C. Liu, J. Fang, M. Wang, J. Chen, J. Zhang, C. Mao, S. Xu, *Langmuir* **2010**, *26*, 1278.
[16] O. Veiseh, J. W. Gunn, M. Q. Zhang, *Adv. Drug Delivery Rev.* **2010**, *62*, 284.
[17] L. Wang, W. Zhao, W. Tan, *Nano Res.* **2008**, *1*, 99.
[18] R. Ke, W. Yang, X. Xia, Y. Xu, Q. Li, *Anal. Biochem.* **2010**, *406*, 8.
[19] Y. Piao, A. Burns, J. Kim, U. Wiesner, T. Hyeon, *Adv. Funct. Mater.* **2008**, *18*, 3745.
[20] V. Biju, T. Itoh, M. Ishikawa, *Chem. Soc. Rev.* **2010**, *39*, 3031.
[21] Z. Krpetic, P. Nativo, F. Porta, M. Brust, *Bioconjugate Chem.* **2009**, *20*, 619.
[22] R. Bardhan, W. Chen, C. Perez-Torres, M. Bartels, R. M. Huschka, L. Zhao, E. Morosan, R. Pautler, A. Joshi, N. J. Halas, *Adv. Funct. Mater.* **2009**, *19*, 3901.
[23] W. Lian, S. A. Litherland, H. Badrane, W. H. Tang, D. H. Wu, H. V. Baker, P. A. Gulig, D. V. Lim, S. G. Jin, *Anal. Biochem.* **2004**, *334*, 135.
[24] A. Burns, H. Ow, U. Wiesner, *Chem. Soc. Rev.* **2006**, *35*, 1028.
[25] M. Qhobosheane, S. Santra, P. Zhang, W. Tan, *Analyst* **2001**, *126*, 1274.
[26] S. Megelski, G. Calzaferri, *Adv. Funct. Mater.* **2001**, *11*, 277.
[27] A. Z. Ruiz, D. Brühwiler, T. Ban, G. Calzaferri, *Monatsh. Chem.* **2005**, *136*, 77.
[28] D. Brühwiler, G. Calzaferri, *Microporous Mesoporous Mater.* **2004**, *72*, 1.
[29] S. Megelski, A. Lieb, M. Pauchard, A. Drechsler, S. Glaus, C. Debus, A. J. Meixner, G. Calzaferri, *J. Phys. Chem. B* **2001**, *105*, 25.
[30] R. Ferrini, O. Nicolet, S. Huber, L. Zuppiroli, S. Chappellet, C. Lovey, J. Perrenoud, M. Pauchard, *J. Appl. Phys.* **2010**, *107*, 114323.
[31] G. Calzaferri, S. Huber, H. Maas, C. Minkowski, *Angew. Chem. Int. Ed.* **2003**, *42*, 3732.
[32] G. Calzaferri, K. Lutkouskaya, *Photochem. Photobiol. Sci.* **2008**, *7*, 879.
[33] P. Simoncic, T. Armbruster, *Microporous Mesoporous Mater.* **2005**, *81*, 87.
[34] M. Busby, C. Blum, M. Tibben, S. Fibikar, G. Calzaferri, V. Subramaniam, L. De Cola, *J. Am. Chem. Soc.* **2008**, *130*, 10970.
[35] K. B. Yoon, *Acc. Chem. Res.* **2007**, *40*, 29.
[36] S. Huber, G. Calzaferri, *Angew. Chem. Int. Ed.* **2004**, *43*, 6738.
[37] D. Brühwiler, G. Calzaferri, *C. R. Chim. Acad. Sci. Paris* **2005**, *8*, 391.
[38] M. Busby, H. Kerschbaumer, G. Calzaferri, L. De Cola, *Adv. Mater.* **2008**, *20*, 1614.
[39] Z. Popovi , M. Otter, G. Calzaferri, L. De Cola, *Angew. Chem. Int. Ed.* **2007**, *46*, 6188.
[40] C. Strassert, M. Otter, R. Q. Albuquerque, A. Höne, Y. Vida, B. Maier, L. De Cola, *Angew. Chem. Int. Ed.* **2009**, *48*, 7928.
[41] M. M. Tsotsalas, K. Kopka, G. Luppi, S. Wagner, M. P. Law, M. Schäfers, L. De Cola, *ACS Nano* **2010**, *4*, 342.
[42] Y. Zhang, Y. Liu, J. Kong, P. Yang, Y. Tang, B. Liu, *Small* **2006**, *2*, 1170.
[43] M. Matsui, Y. Kiyozumi, T. Yamaoto, Y. Mizushina, F. Mizukami, K. Sakaguchi, *Chem. Eur. J.* **2001**, *7*, 1555.

[44] a) A. Z. Ruiz, D. Brühwiler, L. Dieu, G. Calzaferri, *Materials Syntheses: A PracticalGuide* (Eds.: U. Schubert, N. Hüsing, R. Laine), Springer, Wien, **2008**, pp. 9–28; b) A. Z. Ruiz, Ph.D. Thesis, University of Bern, Switzerland, **2006**.
[45] M. Busby, A. Devaux, C. Blum, V. Subramaniam, G. Calzaferri, L. De Cola, *J. Phys. Chem. C* **2011**, *115*, 5974.
[46] Z. Popović, M. Tosotsalas, M. Busby, L. De Cola, G. Calzaferri, H.-P. Josel, Patent Application No. WO 2008/052603 A1.
[47] D. Maraldo, R. Mutharasan, *Sens. Actuators B* **2007**, *123*, 474.
[48] J. V. Staros, R. W. Wright, D. M. Swingle, *Anal. Biochem.* **1986**, *156*, 220.
[49] Z. Grabarek, J. Gergely, *Anal. Biochem.* **1990**, *185*, 131.
[50] M. I. Halliday, G. B. Wisdom, *Biochem. Soc. Trans.* **1986**, *14*, 473.
[51] Y. Kishida, B. R. Olsen, R. A. Berg, D. J. Prockop, *J. Cell Biol.* **1975**, *64*, 331.
[52] Thermo Fisher Scientific Inc., "Instructions DSS and BS^3 Crosslinkers", http://www.piercenet.com/instructions/2160418.pdf (last accessed July 2011).
[53] A. Waqar, A. Asif, A. Saad, *Biomedica* **2008**, *24*, 89.

Received: May 17, 2011
Revised: June 17, 2011
Published online: September 28, 2011

